Exosome Surface Display of IL12 Results in Tumor-Retained Pharmacology with Superior Potency and Limited Systemic Exposure Compared with Recombinant IL12 AC

Nuruddeen D. Lewis, Chang Ling Sia, Katherine Kirwin, Sonya Haupt, Gauri Mahimkar, Tong Zi, Ke Xu, Kevin Dooley, Su Chul Jang, Bryan Choi, Adam Boutin, Andrew Grube, Christine McCoy, Jorge Sanchez-Salazar, Michael Doherty, Leonid Gaidukov, Scott Estes, Kyriakos D. Economides, Douglas E. Williams, and Sriram Sathyanarayanan

ABSTRACT

The promise of IL12 as a cancer treatment has yet to be fulfilled with multiple tested approaches being limited by unwanted systemic exposure and unpredictable pharmacology. To address these limitations, we generated exoIL12, a novel, engineered exosome therapeutic that displays functional IL12 on the surface of an exosome. IL12 exosomal surface expression was achieved via fusion to the abundant exosomal surface protein PTGFRN resulting in equivalent potency *in vitro* to recombinant IL12 (rIL12) as demonstrated by IFNγ production. Following intratumoral injection, exoIL12 exhibited prolonged tumor retention and greater antitumor activity than rIL12. Moreover, exoIL12 was significantly more potent than rIL12 in tumor growth inhibition. In the MC38 model, complete responses were observed in 63% of mice treated with exoIL12; in contrast, rIL12 resulted in 0% complete responses at an equivalent IL12 dose. This correlated with dose-dependent increases in tumor antigen–specific $CD8^+$ T cells. Rechallenge studies of exoIL12 complete responder mice showed no tumor regrowth, and depletion of $CD8^+$ T cells completely abrogated antitumor activity of exoIL12. Following intratumoral administration, exoIL12 exhibited 10-fold higher intratumoral exposure than rIL12 and prolonged IFNγ production up to 48 hours. Retained local pharmacology of exoIL12 was further confirmed using subcutaneous injections in nonhuman primates. This work demonstrates that tumor-restricted pharmacology of exoIL12 results in superior *in vivo* efficacy and immune memory without systemic IL12 exposure and related toxicity. ExoIL12 is a novel cancer therapeutic candidate that overcomes key limitations of rIL12 and thereby creates a therapeutic window for this potent cytokine.

Introduction

For more than 2 decades, recombinant cytokines have been investigated for cancer immunotherapy to stimulate antitumor immune responses. The interferons (IFNs) were the first class of cytokines approved for cancer treatment with IFNα2 approved for hairy cell leukemia and stage IIB/III melanoma (1). Subsequently, IL2 therapy was approved for metastatic melanoma and renal cell carcinoma (2). Further clinical development of these cytokines has been severely hampered by poor patient tolerability, including constitutional symptoms, fever, capillary leak, and mortality in some settings. This poor tolerability reflects the fact that these highly potent immune activators are naturally released in precisely controlled and locally compartmentalized ways and do not typically appear in high systemic concentrations as seen with therapeutic administration.

IL12 is part of a family of heterodimeric cytokines originally identified in the supernatant of transformed B cells and composed of 35-kDa and 40-kDa subunits. IL12 signals through a heterodimeric receptor complex present on T cells and NK cells via STAT4-mediated signaling and potently induces IFNγ production and Th1 polarization through induction of the transcription factor T-bet in $CD4^+$ and $CD8^+$ T cells (3). IL12 can also repolarize M2 immunosuppressive macrophages in the tumor microenvironment into immunostimulatory M1 macrophages via local IFNγ production (4). Dendritic cells, monocytes, macrophages, B cells, and neutrophils release IL12 following induction of innate immune pathways (3). These data led investigators to explore the activity of IL12 in numerous preclinical cancer models and single-agent activity mediated via immune mechanisms was documented in several murine tumor models (5–7).

These promising preclinical experiences prompted the testing of rIL12 in patients with cancer (8, 9). Early studies with rIL12 demonstrated only modest single-agent activity in some malignancies, including cutaneous T-cell lymphoma (10), Kaposi sarcoma (11), renal cell carcinoma (12), and melanoma (12). However, like the IFNs and IL2 described above, when IL12 is given systemically, patients exhibited substantial toxicity, including flu-like symptoms, lymphopenia, gastrointestinal and hepatic toxicity, and it resulted in two deaths in early dose-escalation trials (13, 14). These dose-limiting toxicities were mainly associated with the systemic IFNγ production and NK cell activation. Although local/regional dosing and schedule exploration of rIL12 has resulted in modest improvements of the therapeutic window, tolerability remains challenging with systemic dosing (15). Recent studies using local IL12 administration within the tumor microenvironment (16, 17) have produced promising initial results and demonstrated potentially wider therapeutic windows. The use of plasmid DNA encoding IL12 (16) or viral delivery of IL12 (18) has shown

Codiak BioSciences Inc., Cambridge, Massachusetts.

Note: Supplementary data for this article are available at Molecular Cancer Therapeutics Online (http://mct.aacrjournals.org/).

Corresponding Author: Sriram Sathyanarayanan, Codiak BioSciences, 35 Cambridge Park Dr., 5th Floor, Cambridge, MA 02140. Phone: 617-949-4218; E-mail: sriram.sathy@codiakbio.com

Mol Cancer Ther 2021;20:523–34

doi: 10.1158/1535-7163.MCT-20-0484

promise and have provided early clinical proof of concept. However, inconsistent exposure and durability of IL12 production in these studies may yield low levels of antitumor activity and the potential for systemic toxicity upon IL12 extravasation, particularly given the inability to precisely control expression levels using these modalities.

Exosomes are natural cellular messengers composed of 30- to 200-nm membrane-delimited particles released by all cells. The studies reported here describe a unique exosome-based approach to locally deliver IL12 via intratumoral (IT) dosing in the tumor microenvironment, resulting in robust antitumor activity in preclinical tumor models, prolonged tumor retention, and a lack of systemic exposure. Using our proprietary methods for displaying functional biomolecules on the surface of exosomes (19), we have created a therapeutic candidate, exoIL12, which allows for precise IL12 dosing and retention in the tumor microenvironment following local administration. Preclinical studies in mice and nonhuman primates (NHPs) confirm the unique pharmacodynamic (PD) effects of exoIL12 resulting in a wide therapeutic window and greater apparent potency than the parent rIL12 *in vivo*. We believe the properties of exoIL12 will allow the full potential of IL12 to be realized in human cancers.

Results

Design and production of exosomes with functional, surface-displayed IL12

We recently reported on the development of a platform technology, engEx, which allows for the display of biologically active macromolecules on the surface or within the lumen of exosomes (19). Prostaglandin F2 Receptor Negative Regulator (PTGFRN) is a type I membrane protein abundantly expressed on the exosome surface and serves as a scaffold to display IL12 on the exosome membrane (**Fig. 1A**). We constructed plasmids with the coding sequence of PTGFRN fused to a single-chain version of human IL12 consisting of the p35 and p40 subunits connected by a flexible linker. Clonal cell lines producing engineered exosomes were derived, and high-producing clones were selected for cell culture scale-up, exosome isolation, and biochemical and biological characterization as described previously (19). Because human IL12 does not cross-react with the mouse IL12 receptor, a similar construct with mouse p35 and p40 subunits fused to human PTGFRN, was also generated and stable cell lines expressing mouse exoIL12 were established. IL12 expression on the purified exosomes was confirmed by Western blot analysis using an anti-IL12 antibody, which showed a single predominant PTGFRN-IL12 fusion protein of the expected size (Supplementary Fig. S1). In addition, IL12 was confirmed to be on the outside of the exosomes using bead-based pull-down followed by flow cytometry using anti-IL12 and anti-CD81 antibodies (Supplementary Fig. S6). The exoIL12 exosomes were of a similar size range as native exosomes and the integrity of the exosomes was further confirmed by electron microscopy (Supplementary Fig. S1). Immunoblot analysis showed enrichment of frequently reported exosome markers TSG101, ALIX, and SDCBP as well as other tetraspanin members, such as CD9, CD63, and CD81 (20), were observed in the exoIL12 exosomes further confirming the identity of these nanoparticles.

We compared the relative potency of exoIL12 with rIL12 in the ability to induce IFNγ production from T cells and NK cells *in vitro*. Purified exosomes displaying mouse or human IL12 (exoIL12) were isolated and IL12 levels were quantitated. Human rIL12 and exoIL12 induced IFNγ production from peripheral blood mononuclear cells (PBMCs) stimulated with anti-CD3 in a dose-dependent manner (**Fig. 1B**). No IFNγ production was observed in the absence of anti-CD3 stimulation. This result is consistent with previous reports (21) wherein anti-CD3 treatment increases IL12 receptor levels making them responsive to IL12. The concentration of IL12 required to induce half-maximal release of IFNγ (EC_{50}) for human rIL12 (0.237 ng/mL) and exoIL12 (0.195 ng/mL) were not significantly different (**Fig. 1C**) with data from 13 to 18 individual PBMC donors. Similar results were observed with IL1β-stimulated NK cells (Supplementary Fig. S2). A similar assay format was used to assess murine exoIL12 using anti-CD3 stimulated mouse splenocytes as target cells for IFNγ induction. The EC_{50} values of murine rIL12 (0.090 ng/mL) and exoIL12 (0.054 ng/mL) were not significantly different with data from 10 to 18 donors (**Fig. 1D**). We also assessed the relative potency of human rIL12 and exoIL12 in cultures of cynomolgus monkey PBMCs stimulated by anti-CD3 and, likewise, saw no significant differences in potency when assessing IFNγ production (**Fig. 1E**). These data collectively demonstrate that exosome displayed murine and human IL12 exhibit full biological activity comparable with the recombinant version of the cytokine with no loss in specific activity.

ExoIL12 induces more potent antitumor immunity as compared with rIL12 in murine tumor models

We conducted a series of murine preclinical studies in animals bearing MC38, CT26, and B16F10 tumors. We compared the relative activity of murine rIL12 and exoIL12 across a dose range with every other day dosing IT for three doses. In both MC38 and CT26 models, exoIL12 showed pronounced inhibition of tumor growth at 100 ng per dose as compared with an equivalent dose of rIL12 (**Fig. 2A**). Tumors continued to grow in the rIL12-treated group at the 100-ng dose [8% tumor growth rate inhibition (%TGRI) in MC38 and 5.1% in CT26], and no complete responses (CRs) were observed. ExoIL12 showed dose-dependent effects on tumor growth rates in all three tumor models at doses of 1, 10, or 100 ng (**Fig. 2A**). At the 100-ng dose level, CRs were observed in 63% of mice with MC38 (96.4% TGRI) and 60% of mice with CT26 (72.8% TGRI; **Fig. 2A**). Modest tumor growth inhibition was observed in the B16F10 tumor model with three doses (100 ng) of exoIL12 (33.2% TGRI). This tumor growth inhibition was further enhanced by continuing the exoIL12 therapy for up to eight doses (57.4% TGRI; **Fig. 2A**).

We evaluated the systemic effect of IL12 on the expansion of tumor antigen-specific T-cell responses in the spleen of MC38 tumor–bearing mice at the end of the study. A dose-dependent increase in p15e (a tumor neo-epitope; ref. 22) peptide tetramer–reactive $CD8^+$ T cells was observed in the spleens of mice treated with exoIL12, but not in the spleens of control animals or animals receiving 100 ng of rIL12 (**Fig. 2B**). The expansion of tumor antigen–specific T cells supports the development of systemic antitumor immunity.

Tumor rechallenge studies were also carried out in the MC38 model to assess the development of immunologic memory in animals treated with effective doses of exoIL12. As seen in prior studies, 100 ng of rIL12 dosed IT was ineffective at tumor control, whereas 100 ng of exoIL12 dosed IT demonstrated potent tumor growth inhibition resulting in 50% CRs and 86.9% TGRI (**Fig. 2C**). On day 37, animals with a CR ($n = 4$) to the initial tumor were rechallenged with an inoculum of MC38 cells in the opposing flank. Mice that achieved a CR from the primary tumor uniformly rejected growth of the secondary MC38 cells. In contrast, uniform tumor growth was observed in naïve mice (**Fig. 2C**). These results demonstrate a potent immunologic memory response induced by exoIL12 treatment. The development of immunologic memory was further confirmed by isolating splenocytes and assessing the percentage of p15e tetramer–positive $CD8^+$ cells. Spleens of exoIL12-treated mice had substantial expansion of antigen-specific

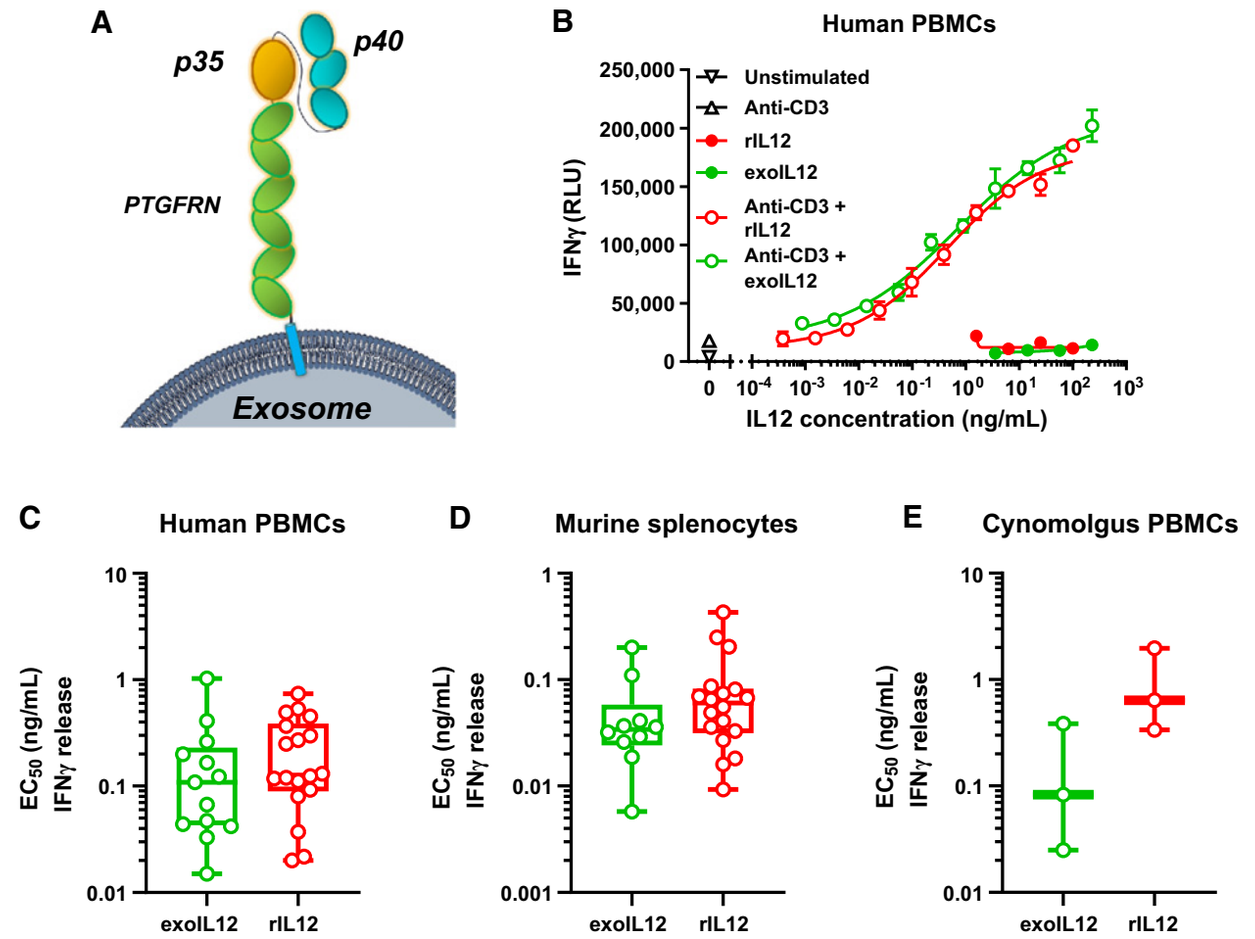

Figure 1.

Design and production of exosomes with functional, surface-displayed IL12. **A,** ExoIL12 is an engineered exosome that displays single-chain IL12 on the membrane glycoprotein PTGFRN on the surface of exosome. **B,** Representative dose–response curves of IFNγ secretion from anti-CD3–stimulated human PBMCs after treatment with dose titrations of exoIL12 or rIL12. **C,** EC_{50} values derived from the graphs of IFNγ production from anti-CD3–stimulated human PBMCs after treating with exoIL12 ($n = 13$) or rIL12 ($n = 13$). **D,** EC_{50} values derived from the graphs of IFNγ production from anti-CD3–stimulated murine splenocytes after treating with exoIL12 ($n = 10$) or rIL12 ($n = 18$). **E,** EC_{50} values derived from the graphs of IFNγ production from anti-CD3–stimulated cynomolgus PBMCs after treating with exoIL12 or rIL12 ($n = 3$). Data were analyzed with unpaired *t* test for human and murine and a paired *t* test for cynomolgus. There were no statistically significant differences between the two groups in all three species.

$CD8^+$ T cells (Supplementary Fig. S3A). The functionality of these antigen-specific immune responses was confirmed by IFNγ production following stimulation with an MC38 protein lysate by ELISpot analysis that showed expansion of antigen-specific IFNγ-secreting cells in the rechallenged animals but not seen in control animals (Supplementary Fig. S3B).

The requirement for $CD4^+$ T cells, $CD8^+$ T cells, and NK cells in mediating antitumor responses was further characterized with antibody depletion studies. Following tumor implantation, the $CD4^+$ T cells, $CD8^+$ T cells, and NK cells were depleted by treatment with depleting antibodies 2 days before the initiation of exoIL12 IT treatment. Robust tumor growth inhibition was observed in the exoIL12-treated isotype control group. In contrast, all tumor growth inhibition was reversed in the anti-CD8 antibody–treated group (**Fig. 2D**). Anti-CD4 treatment alone reduced the tumor growth in this model suggesting potential depletion of regulatory T cells. The exoIL12-treated group in the presence of anti-CD4 showed similar tumor growth as the corresponding control group (Supplementary Fig. S4A). In the anti-NK1.1 antibody–treated group, tumor growth inhibition by exoIL12 was unaffected (**Fig. 2D**). Confirmation of the cellular depletion was observed in the spleen (Supplementary Fig. S4B). These data suggest that the $CD8^+$ T cells play a central role in mediating exoIL12 antitumor activity, whereas NK cells do not play an important role in controlling tumor growth.

To further explore the mechanistic difference in antitumor efficacy observed between exoIL12 and rIL12 in the MC38 model, we examined the $CD8^+$ T cell, NK cell, and M1 and M2 polarized macrophage infiltrate in the tumor at the end of the study by IHC or *in situ*-hybridization (ISH; **Fig. 3**). In addition, IFNγ levels, cytotoxic T cells, as estimated by $CD8^+$/granzyme double-positive cells, and endothelial cells ($CD31^+$) were examined in the tumor. In the exoIL12 treated group, increased infiltration of $CD8^+$ T cells (4-fold vs. 1.2-fold), $NCR1^+$ NK cells (11.3-fold vs. 0.6-fold), and cytotoxic T cells (7.9-fold vs. 1.2-fold) was observed as compared with the rIL12-treated group.

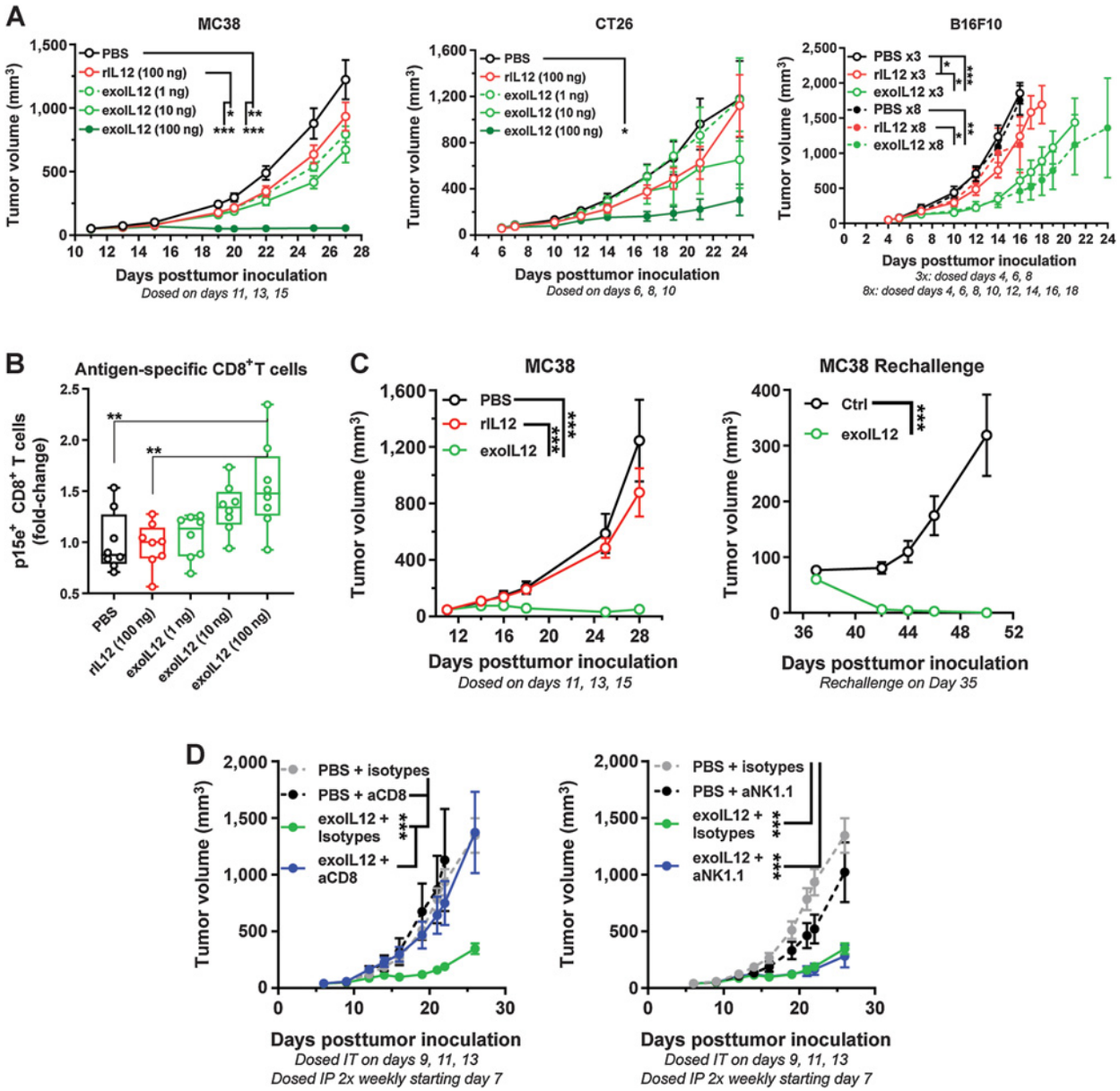

Figure 2.

ExoIL12 induced antitumor immunity in mouse models. **A,** Tumor growth means ± SEM are displayed for tumor volumes from the various treatment groups over time. Mice were dosed three times IT for MC38 ($n = 8$) and CT26 ($n = 10$). Mice were dosed either three or eight times IT for B16F10 ($n = 5$). **B,** Spleens were collected at the end of the MC38 study and assessed for p15e$^+$ MC38-specific CD8$^+$ T cells using tetramers ($n = 8$). **C,** Mean ± SEM is displayed for tumor volumes from the various treatment groups over time in the MC38 model. Mice were dosed (100-ng exoIL-12) three times IT ($n = 8$). Mean ± SEM is shown for the MC38 rechallenge. Mice with complete responses ($n = 4$), along with naïve age-matched mice ($n = 10$), were rechallenged with MC38 cells injected subcutaneously in the opposite flank. **D,** Tumor growth (means ± SEM) are displayed for MC38 tumor volumes. Mice were dosed three times IT with PBS or exoIL12 (100 ng). Mice were also dosed intraperitoneally throughout the duration of the study with antibodies to deplete cell types as shown (***, $P < 0.001$; **, $P < 0.01$; *, $P < 0.05$ by one-way ANOVA with Tukey multiple comparison test).

Furthermore, IFNγ mRNA levels were also 13.9-fold higher as assessed by RNAScope (**Fig. 3A** and **B**). These results were consistent with the greater effect on tumor growth of exoIL12. We next evaluated the effect on tumor vasculature by evaluating CD31$^+$ endothelial cells. There was no significant difference in the number of CD31$^+$ cells; however, lowest number of CD31$^+$ cells was observed in the exoIL12-treated group. Predominantly in the tumor margins, we also observed an increase (9.25-fold) in the number of F4/80$^+$ macrophages in tumors treated with exoIL12; in contrast, there was no observed increase with rIL12 treatment (**Fig. 3C** and **D**). We determined the polarization state of these macrophages using inducible nitric oxide synthase (iNOS), a marker for M1 polarization, and arginase I (Arg1) a marker for M2

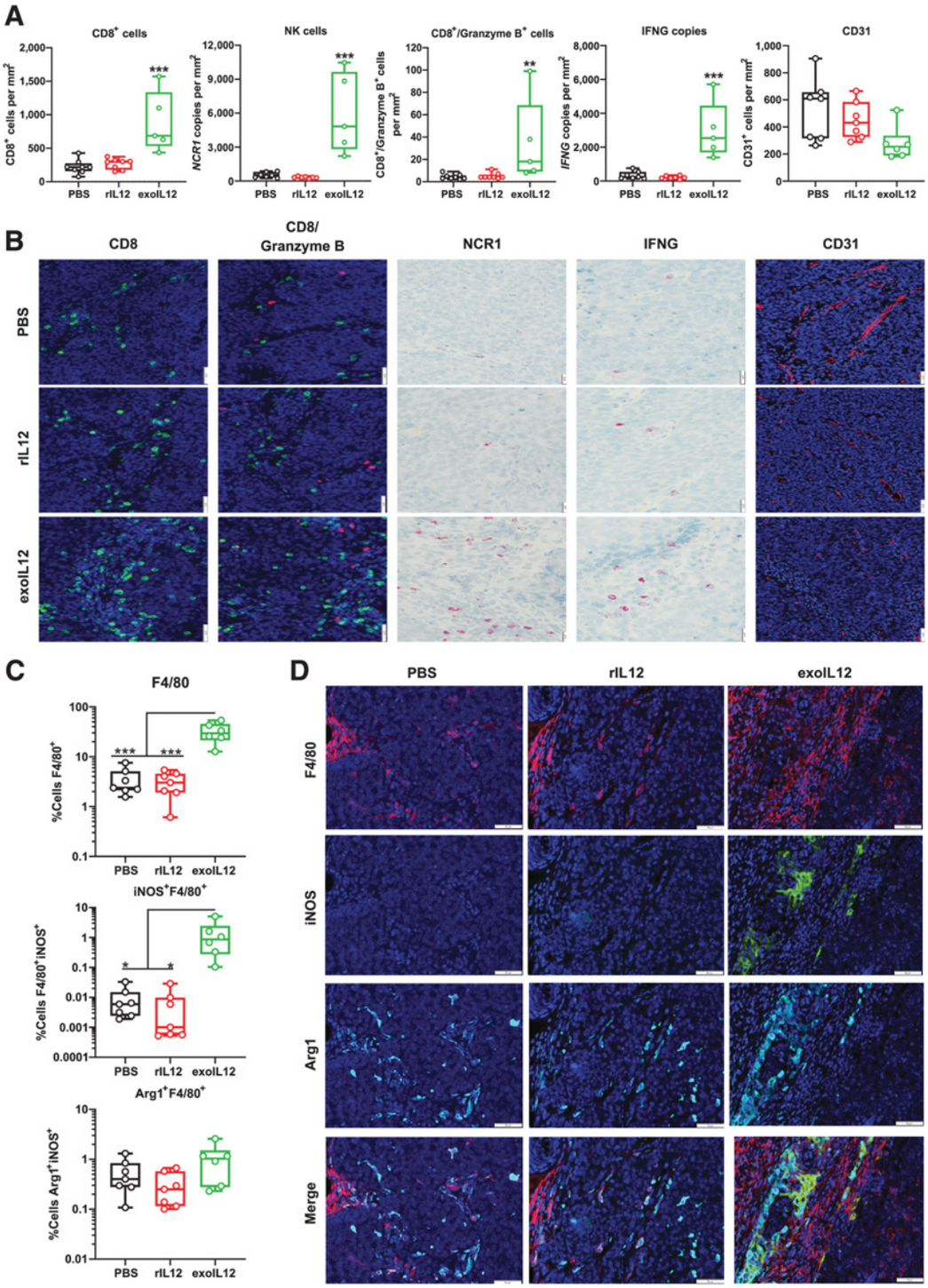

Figure 3.

ExoIL12 induced tumor infiltration of CD8$^+$ cells, NK cells, and M1 macrophages. **A,** Quantitation of CD8$^+$ cells, NK cells (NCR1), CD8$^+$/granzyme B$^+$, IFNG mRNA copies, and CD31$^+$ cells performed by IHC and ISH in MC38 tumors at the end of the study referenced in **Fig. 2C**. **B,** Representative images for the quantitation shown in **A**. **C,** Quantitation of tumor-infiltrating macrophages (F4/80$^+$) and assessment of M1 (iNOS$^+$) or M2 (Arg1$^+$) polarization performed by IHC in MC38 tumors at the end of the study referenced in **Fig. 2C**. **D,** Representative images for the quantitation shown in **C** (***, $P < 0.001$; **, $P < 0.01$; *, $P < 0.05$ by one-way ANOVA with Tukey multiple comparison test).

Table 1. Intratumoral exposure in MC38 tumors.

Treatment	Dose	AUC_{last} (pg/tumor *hr)	C_{max} (pg/tumor)	T_{max}
Murine exoIL12	1 ng	661	53	0
Murine exoIL12	10 ng	1,072	539	0
Murine exoIL12	100 ng	1,9479	6034	0
Murine rIL12	100 ng	1,875	1502	0

Abbreviations: AUC_{last}, area under curve up to the last timepoint; C_{max}, maximum observed concentration; T_{max}, timepoint for maximum observed concentration.

polarization. In the tumor margins, more $F4/80^+$/$iNOS^+$–positive macrophages were observed with exoIL12 treatment as compared with the control group (152-fold increase). No such increase was observed in the rIL12-treated group. Also, there was no difference in the amount of $Arg1^+$/$F4/80^+$ macrophages. These data suggest that exoIL12 induces an influx of $F4/80^+$ cells that are M1 polarized.

Tissue retention of exoIL12 promotes differential pharmacology to rIL12

Previous work with exosome delivery of a STING agonist has shown that tissue retention can widen the therapeutic index and lead to enhanced potency (23). To explore the tissue retention and pharmacodynamic response to exoIL12 or rIL12 treatment, we measured the kinetics of IL12 retention and IFNγ protein levels in the MC38 tumor model upon IT dosing. The results are summarized in **Table 1**. A dose-dependent increase in IL12 exposure was observed. ExoIL12 resulted in approximately 10-fold greater IT exposure (area under curve) as compared with rIL12 at an equivalent dose. The relative magnitude and duration of the pharmacodynamic response as measured by tumor tissue IFNγ levels also showed a significant difference between rIL12 and exoIL12. While the maximal induction of IFNγ was comparable between rIL12 and exoIL12, rIL12 showed a rapid decline in IFNγ by 8 hours. In contrast, exoIL12 treatment resulted in prolonged production of IFNγ, which was detectable up to 48 hours (**Fig. 4A**). In the serum, there were no detectable increases observed in IL12 or IFNγ at 0.5, 3, 8, 24, and 48 hours postdosing. Additional serum cytokines were also measured including TNFα, IL6, and MCP-1 and no dose-dependent increases were observed.

To confirm the tissue-retained pharmacology of exoIL12, we assessed tumor retention and pharmacodynamic responses in the B16F10 model, which is poorly infiltrated with T cells. As shown in **Fig. 2A**, this model is also responsive to 100 ng of exoIL12, but not rIL12. Like the findings in the MC38 tumor model, enhanced tumor retention of exoIL12 was observed. The single-dose kinetic study following IT dosing of comparable amounts of rIL12 (100 ng) or exoIL12 (100 ng) resulted in 15-fold enhanced intratumoral exposure with exoIL12 as compared with rIL12. Similar to the MC38 tumor model, a rapid loss of rIL12 was observed from the tumor with near complete loss by 3 hours postinjection (**Fig. 4B**). In contrast, exoIL12 was retained and detectable as much as 48 hours after injection (**Fig. 4B**). In addition, a prolonged IFNγ response in the tumor was also observed. Although the maximal induction of IFNγ was comparable between rIL12 and exoIL12 treated animals with maximal levels at 12 hours after injection, rIL12 showed a rapid decline in IFNγ by 24 hours (**Fig. 4B**). In contrast, even at 48 hours postinjection, exoIL12-induced IFNγ levels were near maximal and exhibited a prolonged pharmacodynamic response as compared with rIL12 (**Fig. 4B**).

Previous studies have demonstrated accumulation of IFNγ in serum following continuous dosing with rIL12 (15). Continuous dosing from day 7 to day 15 of either rIL12 or exoIL12 in B16F10 tumor-bearing mice resulted in tumor growth inhibition by both agents (Supplementary Fig. S5). Forty-eight hours after the last dose (day 17), we collected both tumor tissue and serum to assess IL12 accumulation in both compartments. Consistent with the single-dose kinetic studies, in the tumor tissue significantly more IL12 was detected in the exoIL12-treated group as compared with the rIL12-treated mice (**Fig. 4C**). Because of continuous dosing, the tumor tissue contained similar levels of IFNγ in both rIL12 and exoIL12 groups. Recombinant IL12 induced substantial levels of serum IFNγ consistent with prior studies (15) and likely reflects the short observed residence time of IL12 in the tumor (**Fig. 4C**). In contrast, administration of exoIL12 did not result in detectable IFNγ in the serum despite the prolonged kinetics of local IFNγ elicited in response to exoIL12 (**Fig. 4C**). These results confirm the prolonged tumor retention of exoIL12 in two immunologically diverse tumor types, MC38 (T-cell rich) and B16F10 (T-cell poor).

Tissue-localized pharmacology and lack of systemic IL12 exposure with subcutaneous exoIL12 in cynomolgus monkeys

As reported previously (15) and confirmed in **Fig. 1C**, human IL12 is active on cynomolgus monkey cells. We have previously shown with imaging of Zr89-labeled exosomes that they remain highly localized after subcutaneous injection (24). We sought to examine whether the local pharmacology described in mice with exoIL12 would be observed upon subcutaneous administration to NHP. NHP were dosed subcutaneously with increasing doses up to a 5-μg dose of exoIL12. Both serum and punch biopsies from the injection site were collected and IL12, IFNγ, and other cytokines as well as IFNγ-regulated gene expression changes were measured. Previously published studies of subcutaneous administration of rIL12 at comparable doses with those used in the current studies showed significant induction of circulating inflammatory cytokines, including IL12 and IFNγ (25). ExoIL12 treatment resulted in dose-dependent increases in levels of IL12 at the injection site with prolonged exposure up to 7 days (**Fig. 5A**). In contrast, analysis of plasma samples at any time point post subcutaneous dosing of exoIL12 did not result in detectable IL12 above the vehicle control levels (**Fig. 5B**). There was also no observed dose-dependent induction of any of the panel of cytokines assessed (MCP-1, IL8, GM-CSF, IFNγ, TNFα, IL23, IFNβ, IL17α, IL12p40, IL1β, IP-10, and IL6) in the plasma of exoIL12-treated NHPs (Supplementary Tables S1 and S2). A dose-dependent induction of mRNA was observed by NanoString analysis on day 7 postdosing with 62 genes of 770 assessed showing significant upregulation in the 5-μg exoIL12 group (**Fig. 5C**). We specifically looked at CXCL10 and CD86, genes known to be induced by IFNγ, and saw dose-dependent upregulation in these genes at this timepoint (**Fig. 5D**). These data support the observations in the mouse models that show significant local induction of immunomodulatory signals at the injection site and retention of exoIL12 at the site of injection without systemic exposure.

Discussion

During the last decade, renewed interest in IL12 has resulted in a number of attempts to expand the therapeutic window of this highly potent cytokine without exacerbating toxicity. Here, we demonstrate an exosome-based approach to locally deliver IL12 via IT dosing in the tumor microenvironment, resulting in robust antitumor activity in

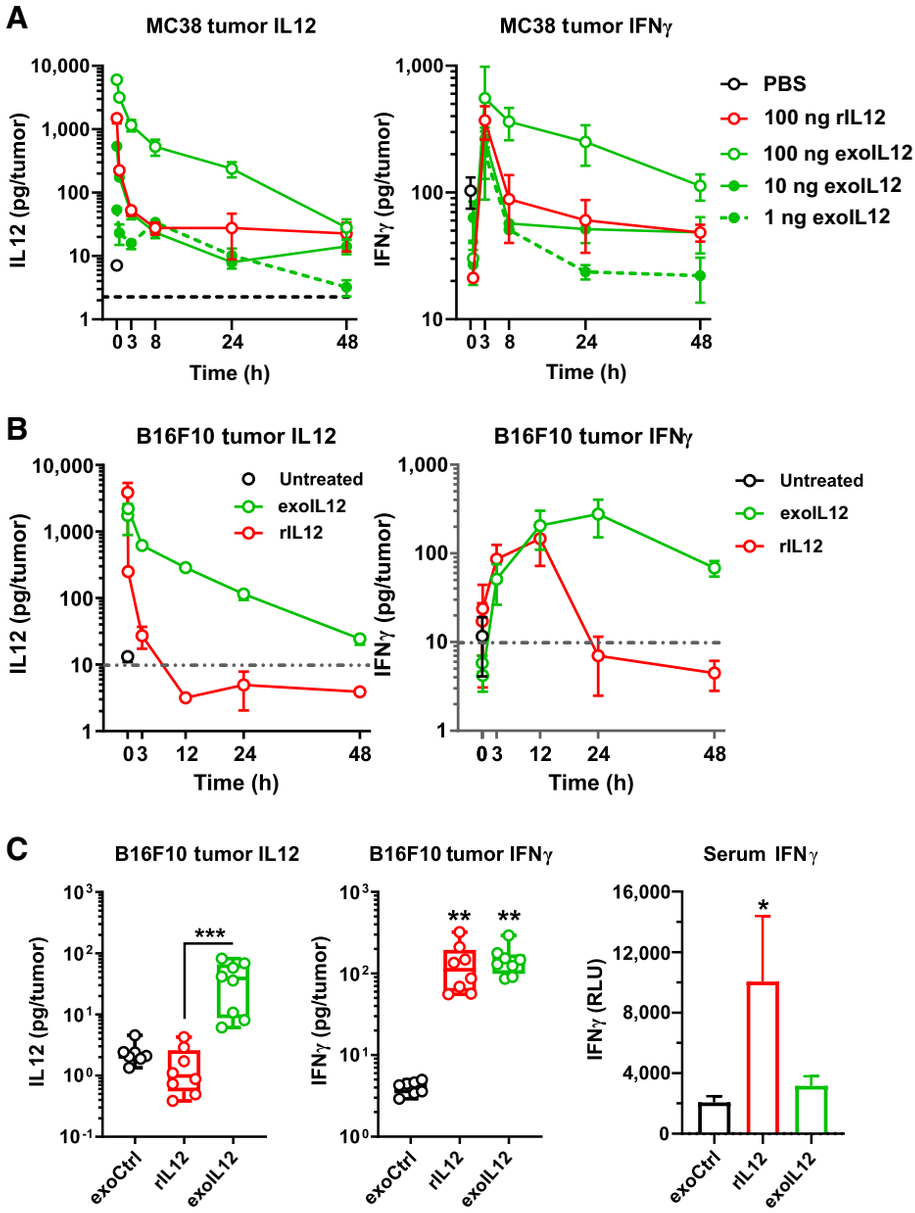

Figure 4.

Increased tumor retention leading to sustained PD of exoIL12 after IT dosing. **A,** MC38 subcutaneous tumors were injected IT with exoIL12 (100 ng, 10 ng, or 1 ng) or rIL12 (100 ng) and assayed for IL12p70 and IFNγ levels at specified timepoints. Time zero samples were generated by injection of tumors *ex vivo*. $N = 3$ mice per group and timepoint. Data are shown as the total amount of cytokine in pg in the entire tumor. **B,** B16F10 subcutaneous tumors were injected IT with exoIL12 (100 ng) or rIL12 (100 ng) and assayed for IL12p70 and IFNγ levels at specified timepoints. Time zero samples were generated by injection of tumors *ex vivo*. $N = 3$ mice per group and timepoint. Data are shown as the total amount of cytokine in pg in the entire tumor. **C,** Mice bearing B16F10 subcutaneous tumors and B16F10 lung metastases were dosed IT into flank tumor once daily for nine total doses ($n = 8$). IT IL12p70, IT IFNγ, and serum IFNγ assessed on day 17 postinoculation are shown ($n = 8$; ***, $P < 0.001$; **, $P < 0.01$; *, $P < 0.05$ by one-way ANOVA with Tukey multiple comparison test).

preclinical tumor models, prolonged tumor retention, and a lack of systemic exposure.

The inherent challenges of localizing potent cytokines to the tumor tissue has prompted multiple approaches that involve local delivery of rIL12, autologous cell therapies to deliver IL12, gene therapy for local delivery, plasmid delivery by *in situ* electroporation, and fusion to tumor-targeting antibodies or proteins (26–30). The goal of these approaches was not only to address the challenges of systemic dosing of IL12 and the pronounced tolerability issues, but also to localize the Th1-inducing effects of IL12 in the tumor microenvironment to reverse the immunosuppressive milieu. Recent reports with these approaches have been encouraging with preliminary data showing single-agent activity in a number of tumor types including cutaneous T-cell lymphoma, melanoma, Merkel cell carcinoma, and glioma with acceptable safety (31–33). Despite these promising results, there are still significant challenges. The common challenge for local rIL12, viral vector, and plasmid-based delivery is that the release of IL12 can be both local and systemic. IL12 readily extravasates into the circulation and without a mechanism to regulate expression levels and duration of IL12 production, consistent efficacy and safety may prove elusive. Published studies show a high degree of variability in the quantity and duration of IL12 production (32), and local injection of rIL12 has shown an adverse event profile due to minimal retention of rIL12 in the injected tissue (34), which is consistent with earlier experience with systemic dosing. Among the improvements made to cytokines, fusion to large biomolecules such as albumin or polyethylene glycol has been successfully used to extend cytokine persistence in circulation. There have been numerous efforts to improve the therapeutic index of cytokines by targeting. Most commonly, cytokines have been fused to tumor-targeting antibodies or other proteins that bind tumor-associated proteins. However, such fusions, generally, first extend a cytokine's systemic exposure before diffusion into the tumor and, as a

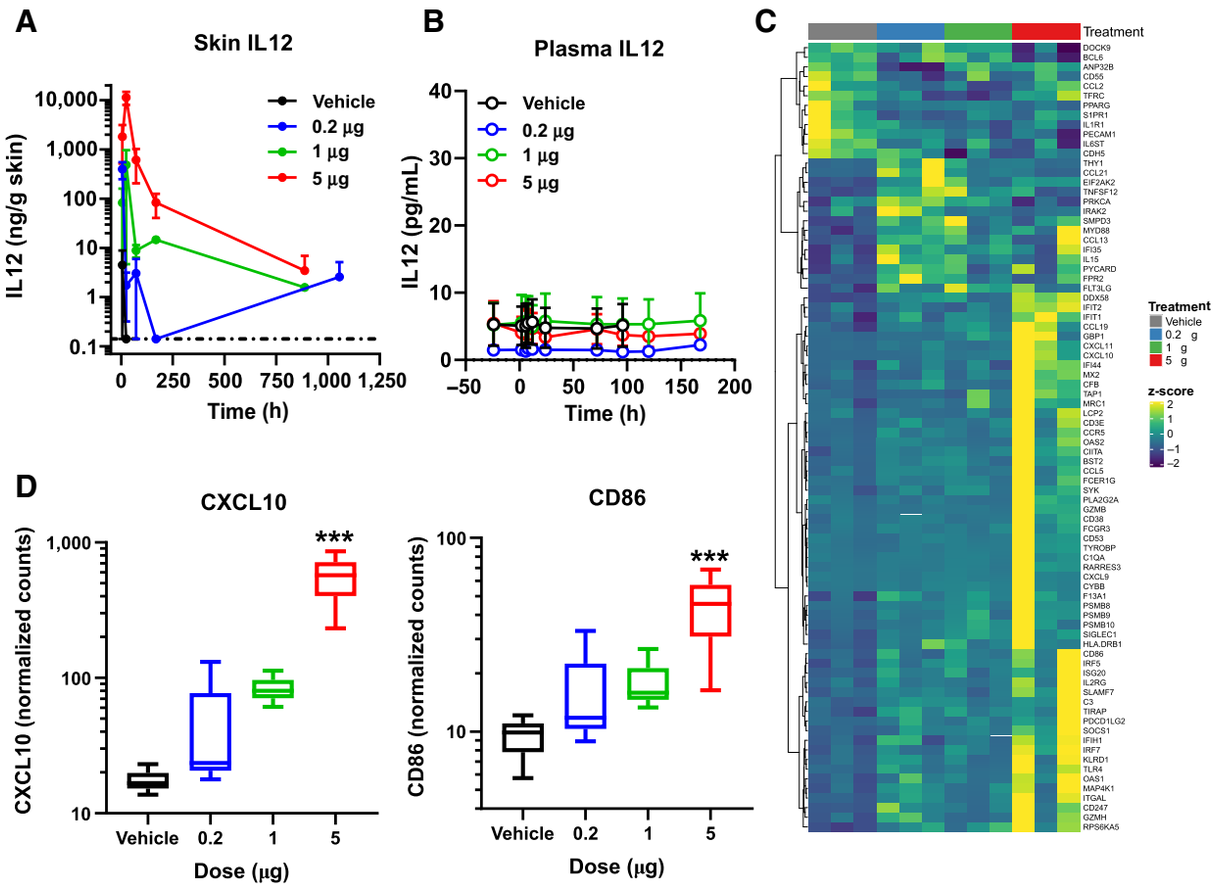

Figure 5.

Localized pharmacology and lack of systemic exposure with subcutaneous exoIL12 in cynomolgus monkeys. Cynomolgus monkeys were injected subcutaneously with vehicle, 0.2, 1, or 5 µg of exoIL12. Human IL12 levels were measured in skin biopsies at 6, 24 hours, day 4, 7, 37 and 44 hours postdosing (**A**), and in plasma (**B**) at predosing, 2, 6, 8, 12, 24 hours, day 3, 4, 5, and 7 postdosing using LEGENDplex NHP Inflammation kit. **C,** Heatmap of gene analysis by NanoString on day 7 postdosing skin biopsies. All genes significantly modulated as compared with the vehicle group using a one-way ANOVA and Dunnett test are shown. **D,** Normalized *CXCL10* and *CD86* gene counts are shown. Both were among the genes that were significantly upregulated with exoIL12.

result, often still suffer from dose-limiting systemic toxicities (27, 28, 30). Although the preclinical investigations of these agents relied on systemic administration, the clinical studies were limited to IT administration with moderate efficacy. However, even upon IT dosing, antibodies also extravasate into systemic circulation leading to cytokine induction (29). IT administration of the fusion of IL12 to the collagen-binding protein lumican prolongs local retention and markedly reduces systemic exposure (30). However, collagen density may vary across multiple tumor types limiting clinical utility of the approach to collagen-rich tumors.

We have recently described methods for engineering exosomes into a drug-delivery platform (19). The tumor retention of exosomes prompted us to explore the development of an engineered exosome displaying functional IL12. The desired phenotype of the therapeutic candidate was expected to allow for precise dosing of active IL12 in the tumor microenvironment. This would maximize exposure of this potent cytokine in the tumor microenvironment and minimize systemic exposure, thus addressing the limitations of many of the approaches for IT or peritumoral dosing described above.

Recent studies have demonstrated that exosomes derived from cells engineered to overexpress IL12 can inhibit tumor growth when administered IT (35). However, the antitumor activity of these engineered MC38-derived exosomes, which relied on stochastic loading of IL12 on to the exosomes, resulted only in modest antitumor activity (35). The exoIL12 candidate described in this manuscript was engineered by fusing the coding sequences of the N-terminus of the exosome membrane protein PTGFRN to the IL12 subunits p35 and p40, stabilized by a flexible linker. Purified engineered exosomes were isolated by discontinuous density gradients from clonal cell culture supernatants and were substantially devoid of contaminating proteins and nucleic acids as described (ref. 19; Supplementary Fig. S1). Functional display of IL12 was confirmed in a series of *in vitro* assays and demonstrated equipotent activity in T-cell and NK-cell activation assays *in vitro*. This was true for human IL12-expressing and murine IL12-expressing exosomes, the latter of which was constructed to allow for preclinical experimentation in mouse syngeneic tumor models.

Comparative activity of rIL12 and exoIL12 was examined in mouse syngeneic tumor models (MC38, CT26, and B16F10) and consistently showed exoIL12 to be significantly more potent (**Fig. 2A**). Mechanism-of-action studies documented several important properties of exoIL12, including prolonged retention of IL12 in the tumor microenvironment, prolonged duration of pharmacodynamics in the tumor

microenvironment, and absence of significant systemic exposure of IL12 (**Fig. 4**). Despite the observed equipotent EC_{50} values of rIL12 and exoIL12 *in vitro*, exosome-mediated tissue retention translated into a wider therapeutic index with robust antitumor activity. Despite local administration into experimental tumors, systemic $CD8^+$ T-cell–mediated immunity was documented with exoIL12, whereas rIL12 administered at comparable levels failed to demonstrate substantial tumor inhibition. Exosomes lacking IL12 failed to induce any impact on tumor growth rate in these models (Supplementary Fig. S5). These data highlight the ability of exoIL12 to allow for precise dosing into the tumor microenvironment, eliciting significant antitumor immunity, and avoiding the systemic production of inflammatory cytokines to widen the therapeutic window.

We further expanded our observations to explore local tissue retention of exoIL12 with studies in NHPs. Although normal NHP is not the same as the tumor microenvironment, it is a surrogate system to allow us to explore our human exosome construct in a relevant species prior to our planned first-in-human studies. Our previous studies with Zr89-labeled exosomes suggested strong tissue retention and minimal migration from a subcutaneous injection site (24). In this study, we explored a single subcutaneous dose of exoIL12 and measured IL12 levels and pharmacodynamic effects induced by IL12 in the local injected tissue as well as in the blood of treated animals. This allowed us to confirm that our human construct in this model behaved similarly to that seen in mouse tumor models, specifically confirming the tissue retention, robust local pharmacodynamic effects, and the absence of induction of inflammatory cytokines in the circulation.

Clinical translation of intratumorally administered therapies is growing rapidly. Various oncolytic viruses and gene-therapy approaches have been administered intratumorally in multiple clinical studies including patients with melanoma, breast cancer, and head and neck cancer (36). This is also expanding into other more visceral tumors such as lung tumors with the issue being the risk benefit to the patient. We believe that the activity of the exoIL12 construct allows for control of IL12 dosing, maximizing exposure to IL12 in the tumor microenvironment, and avoiding systemic exposure to IL12 and therefore can reduce the risk and improve the benefit. Another concern of intratumoral immunotherapy is the effective control of disseminated metastasis. Our results demonstrate the development of durable systemic antitumor responses following local or regional administration. These results suggest that local intratumoral administration may be essential for systemic antitumor immunity. ExoIL12 may allow us to assess the true potential of this cytokine in human tumors, either alone or in combination with other immune modulators, and highlights the potential of exosomes as a versatile drug delivery approach.

Materials and Methods

Cell engineering

B16F10 and CT26.wt cells were purchased from ATCC. MC38 cells were purchased from Kerafast. PCR tests for detection of 21 different pathogens (Impact I from IDEXX) were performed on all cell lines in 2018 (B16F10, Jan; CT26.wt, Nov; MC38, Aug). No testing was performed to authenticate the cell lines. All cell lines were received, thawed, expanded, and banked in antibiotic-free medium in less than 15 passages. The parental cell line used for exosome engineering and production is HEK293SF-3F6 (HEK293) obtained from the National Research Council Canada. HEK293 cells were stably transfected with a plasmid for the overexpression of an engineered fusion protein, human IL12p70, and human PTGFRN. A mouse surrogate was also engineered with murine IL12p70 on human PTGFRN. The accession numbers for the exact sequences used are: Human IL12B or P40: NM_002187, Human IL12A or P35: NM_000882, Human PTGFRN: NM_020440, Murine IL21b or P40: NM_001303244, Murine IL12a or P35: NM_008351.

Exosome isolation

Cell culture harvests were clarified by centrifugation and the clarified conditioned media was filtered, supplemented with $MgCl_2$, and treated with 20 U/mL benzonase (Millipore) overnight. Media was next concentrated 10× by tangential flow filtration and centrifuged for 60 minutes at 133,900 × *g* at 4°C in a 45 Ti fixed-angle rotor in an Optima XE ultracentrifuge. The pellets were resuspended in PBS to a final volume of 3 mL and mixed with 9 mL of 60% iodixanol solution (OptiPrep, Sigma) resulting in a final concentration of 45% iodixanol. Successive layers of lower density iodixanol solutions were carefully pipetted on top of the 45% layer: 9 mL of 30%, 6 mL of 23%, 6 mL of 18%, and 3 mL of PBS. A density gradient was achieved by centrifuging at 150,000 × *g* for 16 hours at 4°C in a swinging-bucket SW 32 Ti rotor. Exosomes were isolated from the interface between the PBS and 18% iodixanol layer by pipetting. An additional low speed spin at 20,000 × *g* for 30 minutes at 4°C was used to remove any contaminating actin and actin-binding protein species. The supernatant was filtered using a 0.22-μm filter and centrifuged at 133,900 × *g* for 3 hours at 4°C. The exosome pellet was resuspended in PBS and frozen at −80°C.

For the studies in cynomolgus monkeys, HEK293 cells were grown in a perfusion bioreactor with the exosome-containing permeate purified with a proprietary process. The purified exosomes were diafiltered into 15-mmol/L sodium phosphate, 5-mmol/L potassium phosphate, 50-mmol/L sodium chloride, 5% (w/v) sucrose, pH 7.2. Exosomes were frozen at ≤−70°C for long-term storage.

Exosome IL12 quantitation

IL12 was quantitated using PerkinElmer AlphaLISA technology with two antibodies specific to different IL12 epitopes. One antibody specific to IL12 p70 (7B12, BioLegend) was chemically conjugated to acceptor beads by reductive amination following vendor recommended protocols. The second antibody specific to IL12 p40 subunit (A15076D, BioLegend) was purchased in biotinylated form. A lyophilized recombinant human IL12 from R&D Biosystems was reconstituted in 1% BSA and used to create a standard curve. All samples and standards were first diluted in range using PerkinElmer's immunoassay buffer to solubilize IL12 from exosomal membranes. The solubilized IL12 was then incubated for an hour with a solution of an anti-IL12 p70 acceptor bead (10 μg/mL) and biotinylated anti-IL12 p40 (1 μg/mL) in a half-area AlphaPlate. Following incubation, a solution of streptavidin donor beads (80 μg/mL) were added and incubated in the dark for 1 hour. An Alpha-enabled microplate reader (BMG Clariostar) was used to excite the donor beads at 680 nm and read the emission wavelength of the acceptor beads between 515 to 520 nm. The concentration of IL12 in exoIL12 was calculated using the signal output of the standard curve.

SDS-PAGE and Western blotting

SDS-PAGE samples were normalized by exosome input (3E+10 per lane) in reducing or non-reducing Laemmli buffer (Bio-Rad), depending on the primary antibody (Supplementary Table S3). Samples were denatured at 95°C for 10 minutes prior to loading into 4% to 20% TGX stain-free precast gels (Bio-Rad). Total protein profile was imaged on a ChemiDoc gel imaging system (Bio-Rad). For Western blot analysis, protein was transferred to a polyvinylidene difluoride membrane using a Trans-Blot Turbo transfer system (Bio-Rad), and blocked in 1%

casein for 1 hour. Primary antibodies were diluted in blocking buffer and incubated with membranes for 1 to 3 hours. Antigens were detected using HRP-conjugated secondary antibodies and Clarity Western enhanced chemiluminescent substrate (Bio-Rad). All blots were imaged on a ChemiDoc Gel Imaging System (Bio-Rad).

Bead-based pull-down and characterization by flow cytometry

Streptavidin-coated magnetic dynabeads (Thermo Fisher Scientific) were coupled with biotinylated anti-IL12 or anti-CD81 antibodies (BioLegend) by incubating 5E+6 beads with 1-μg antibody in the isolation buffer (0.5% BSA/PBS solution) for 1 hour at 4°C with rotation and 10-minute incubation with blocking buffer (2% BSA/PBS solution). 5E+9 particles of exoCtrl or exoIL12 were mixed with 1E+5 anti-IL12 or anti-CD81–coupled beads in the isolation buffer overnight at 4°C with rotation, blocked for 10 minutes with the blocking buffer, and incubated with the fluorescently labeled anti-IL12-APC and anti-CD81-PE antibodies (BioLegend) in the isolation buffer for 30 minutes at 4°C. The labeled beads were washed twice with the isolation buffer, resuspended in the isolation buffer, and analyzed by flow cytometry.

In vitro potency assessment

Human PBMCs were isolated from fresh whole blood using Lymphoprep in SepMate tubes (STEMCELL Technologies). Cells were stimulated with anti-human CD3 (BioLegend clone OKT3) at a final concentration of 1 ng/mL and plated in round-bottom 96-well plates at 200,000 cells per well in RPMI supplemented with 10% FBS. Dose titrations of exoIL12 and rIL12 were prepared and added to the anti-CD3–stimulated PBMCs in a final volume of 200 μL and incubated at 37°C and 5% CO_2. After 4 days, the supernatants were harvested and analyzed for human IFNγ using an AlphaLISA kit according to the manufacturer's protocol (Perkin Elmer). Murine exoIL12 and rIL12 were tested identically using splenocytes isolated from spleen collected from C57BL/6 mice, anti-mouse CD3ε (BioLegend clone 145–2C11), and the Mouse IFNγ AlphaLISA kit. ExoIL12 and rIL12 were tested similarly using cynomolgus frozen PBMCs purchased from Thermo Fisher Scientific. Upon arrival, frozen PBMCs were thawed and rested before being stimulated with 22 ng/mL of anti-monkey CD3 (Mabtech). The supernatants were collected after 5 days to measure IFNγ by using the Cynomolgus IFNγ AlphaLISA Kit. Human NK cells were isolated from fresh whole blood using RosetteSep Human NK Cell Enrichment Cocktail and Lymphoprep in SepMate tubes (STEMCELL Technologies). Cells were stimulated with 10 ng/mL recombinant human IL1β and plated in round-bottom 96-well plates at 5,000 to 15,000 cells per well in RPMI supplemented with 10% FBS. Dose titrations of exoIL12 and rIL12 were prepared and added to the stimulated NK cells in a final volume of 100 μL and incubated at 37°C and 5% CO_2. After 3 days, the supernatants were harvested to measure IFNγ by using the Human IFNγ AlphaLISA kit.

Animals

Five- to 8-week-old female C57BL/6 or BALB/c mice were purchased from Taconic and Jackson Laboratory, respectively. All animals were maintained and treated at the animal care facility of Codiak Biosciences in accordance with the regulations and guidelines of the Institutional Animal Care and Use Committee (CB2017–001).

In vivo mouse tumor models and treatment

Syngeneic tumor models were established by injecting B16F10 (1×10^6 cells to C57BL/6), MC38 (3×10^6 cells to C57BL/6), or CT26.wt (5×10^5 cells to BALB/c) subcutaneously into the right flank of the mouse. When subcutaneous tumors reached an average volume of 50 to 100 mm^3, mice were randomized into groups according to experimental protocol. All studies with rIL12 or exoIL12 treatment were dosed IT. Tumor volume (mm^3) was calculated as $(\text{width})^2 \times (\text{length}) \times 0.5$. Isotype control antibody (10 mg/kg, BioLegend), anti-CD4 (10 mg/kg, BioLegend, Clone GK15), anti-CD8 (10 mg/kg, BioLegend, Clone 53–6.7), and anti-NK1.1 (10 mg/kg, BioLegend, Clone PK136) were dosed intraperitoneally.

Detection of tumor antigen–specific $CD8^+$ T cells

The collected spleens from *in vivo* studies were processed in Ammonium-Chloride-Potassium (ACK) Lysing Buffer to remove red blood cells. Splenocytes were resuspended in RPMI supplemented with 10% FBS and 0.02 mg/mL DNase I Solution. Cells were stained with Live/Dead (AAT Bioquest), MHC I - p15E tetramers (MBL), and surface markers that included CD45 (BD Horizon, clone 30-F11), CD8 (MBL, clone KT15), CD19 (BioLegend, clone 6D5), and NK1.1 (BioLegend, clone PK136). Data were acquired using the CytoFLEX LX flow cytometer (Beckman Coulter) and analyzed by using CytExpert.

Detection of tumor antigen–specific IFNγ-secreting cells

Mouse IFNγ ELISpot^{PLUS} kit (Mabtech) was used to detect tumor antigen–specific IFNγ-secreting cells. Twenty million MC38 cells were treated with five freeze–thaw cycles to generate lysates. Total protein of the cell lysates was measured using Pierce BCA Protein Assay Kit (Thermo Fisher) and lysates were stored at -80°C until needed. Isolated splenocytes from the control and exoIL12-treated groups were resuspended in filtered RPMI supplemented with 10% FBS and plated at 400,000 cells per well in precoated plates provided by the kit. MC38 lysates (10 μg/mL) was used to stimulate the splenocytes in a final volume of 100 μL. Cells were incubated at 37°C and 5% CO_2 for approximately 18 hours before proceeding to the next steps as described in the manufacturer's protocol. Plates were scanned with an automated ELISpot plate reader (AID) and spots were counted using AID ELISpot software.

IHC and ISH

IHC and ISH analysis was performed on tumor samples isolated at the end of the MC38 study reference in **Fig. 2A**. For IHC, slides were mounted using a Vector Lab H1800, stained using the Leica BOND RX, and scanned using the Olympus VS120 all according to the manufacturer's instructions. Image analysis was performed using Halo IF-high plex module. For ISH, the RNAScope assay was performed using the Leica BOND RX, probes were detected using the RNAScope 2.5 LSx Reagent Kit-RED, scanned using the Olympus VS120, and analysis was performed using the Halo ISH 3.0.3 module, all according to the manufacturer's instructions. A full list of antibodies and probes used, along with the vendor, catalog number, and staining conditions, can be found in Supplementary Table S3.

Tumor and skin cytokine measurements

Tumors were homogenized in ceramic bead tubes that contained T-PER tissue protein extraction buffer with Halt protease and phosphatase inhibitor (Thermo Fisher Scientific) by using the Bead Ruptor Elite homogenizer (Omni International) at 5 m/s for 30 seconds. Tumor lysates were collected after the homogenates were centrifuged at 12,000 × *g* for 10 minutes at 4°C. Total protein of the tumor lysates was measured using Pierce BCA Protein Assay Kit (Thermo Fisher Scientific) and the concentration of tumor lysates was adjusted to 1 mg/mL in the extraction buffer with protease and phosphatase

inhibitor before assaying in LEGENDplex Mouse Inflammation Panel (13-plex) with V-bottom plate (BioLegend). Multiple cytokines were measured according to the manufacturer's protocol. Data were acquired using the CytoFLEX LX flow cytometer (Beckman Coulter) and analyzed with LEGENDplex software. Total pg of cytokine per tumor were calculated by multiplying the result from the LEGENDplex software by the dilution factor and total volume of the lysates. Skin biopsies from NHPs were collected postdosing at 6 and 24 hours, and days 4, 7, 37, and 44. The skin biopsies were processed identically as described above and 500 μg/mL of skin lysates were prepared in the extraction buffer with protease and phosphatase inhibitors prior to cytokine measurement. Pharmacokinetic analysis of exoIL12 in NHP skin was carried out using Quantikine ELISA Human IL12p70 Immunoassay (R&D Systems) according to the manufacturer's protocol. Dose titrations of exoIL12 were prepared in normal skin lysates, which was processed from healthy and untreated cynomolgus skin biopsies and used as standard. Skin lysates from the *in vivo* study were further diluted to 200 μg/mL in normal skin lysates prior to the assay. IL12 concentration in ng per g of total protein was calculated and graphed using GraphPad Prism.

Serum and plasma cytokine measurements

Serum was collected from the treated mice at the end of the *in vivo* study for cytokine analysis. IFNγ was measured using the Mouse IFNγ AlphaLISA kit (Perkin Elmer) according to the manufacturer's protocol. Plasma was collected from the treated cynomolgus monkeys at different time points: predosing, 2, 6, 8, 12, 24 hours, day 1, 3, 4, 5, and 7. Multiple cytokines were measured using the LEGENDplex NHP Inflammation Panel (13-plex) with V-bottom Plate (BioLegend) according to the manufacturer's protocol. Data were acquired using the CytoFLEX LX flow cytometer (Beckman Coulter) and analyzed by using LEGENDplex software.

NanoString analysis in skin biopsies from NHP

Skin lysates were mixed with TRIzol solution and total RNA was isolated by using RNeasy Lipid Tissue Mini Kit (Thermo Fisher Scientific), according to manufacturer's instructions. Fifty nanograms of total RNA was incubated overnight with a Reporter Code set and a Capture Probe set from a nCounter NHP Immunology Panel at 65°C. The solution was loaded into a nCounter SPRINT Cartridge and analyzed by a nCounter SPRINT Profiler. Raw files were analyzed by nSolver Analysis Software 4.0 and normalized gene expression levels were obtained.

Statistical analysis

Data were analyzed using Prism software (v. 8.1.0, GraphPad Software). Conditions were considered significantly different for P values less than 0.05. For *in vitro* potency assessment, an unpaired t test (human and murine) or paired t test (cynomolgus) was used. For tumor growth inhibition, one-way ANOVA was used followed by a Tukey *post hoc* test based on the tumor growth rates of individual animals as described by Hather and colleagues (37). The percentage of tumor growth rate inhibition (%TGRI) was calculated using the equation $100 \times [1 - (X)/(\text{mean(control group)})]$. For the IHC, ISH, $p15e^{+}$ $CD8^{+}$ T cells, IT IL12 and IFNγ, and serum IFNγ experiments, a one-way ANOVA with Tukey *post hoc* was performed. Pharmacokinetic analysis was performed using the PKNCA package using the statistical programming language R (38). For the NanoString experiment, a one-way ANOVA with a Dunnett test was used to compare the treatment groups to the vehicle group.

Authors' Disclosures

N.D. Lewis reports personal fees, nonfinancial support, and other from Codiak BioSciences during the conduct of the study; personal fees, nonfinancial support, and other from Codiak BioSciences outside the submitted work; in addition, N.D. Lewis has a patent for US10723782B2 issued. C.L. Sia reports a patent for US10723782B2 issued. S. Haupt reports a patent for preparation of therapeutic exosomes using membrane proteins issued to Codiak Biosciences, Inc. and a patent for engineered extracellular vesicles and uses thereof pending to Codiak Biosciences, Inc. T. Zi reports a patent for US10723782B2 issued; in addition, T. Zi is an employee of Codiak Bioscience. K. Xu reports a patent for US10723782B2 issued. K. Dooley reports a patent for US10723782B2 issued; in addition, K. Dooley is an employee and shareholder of Codiak BioSciences, Inc. A. Boutin reports personal fees from Codiak BioSciences during the conduct of the study. A. McCoy reports a patent for US10723782B2 issued and personal fees (paid employee of Codiak Biosciences Inc). L. Gaidukov reports a patent for US10723782B2 issued. S. Estes reports a patent for US10723782B2 pending. K.D. Economides reports a patent for US10723782B2 issued. D.E. Williams reports other from Codiak BioSciences during the conduct of the study; other from Codiak BioSciences outside the submitted work; in addition, D.E. Williams has a patent for exoIL12 pending and issued. S. Sathyanarayanan reports other from Codiak BioSciences during the conduct of the study; other from Codiak BioSciences outside the submitted work; in addition, S. Sathyanarayanan has a patent for US10723782B2 issued. No disclosures were reported by the other authors.

Authors' Contributions

N.D. Lewis: Conceptualization, data curation, software, investigation, writing–original draft, writing–review and editing. **C.L. Sia:** Resources, investigation, methodology. **K. Kirwin:** Data curation, investigation, methodology. **S. Haupt:** Data curation, methodology. **G. Mahimkar:** Data curation, methodology. **T. Zi:** Data curation, visualization, methodology. **K. Xu:** Conceptualization, data curation, methodology. **K. Dooley:** Conceptualization, data curation, investigation, methodology. **S.C. Jang:** Data curation, investigation, methodology. **B. Choi:** Data curation, methodology. **A. Boutin:** Data curation, methodology. **A. Grube:** Data curation, methodology. **C. McCoy:** Data curation, formal analysis, methodology. **J. Sanchez-Salazar:** Resources, data curation, methodology. **M. Doherty:** Data curation, investigation, methodology. **L. Gaidukov:** Data curation, methodology. **S. Estes:** Supervision, methodology. **K.D. Economides:** Conceptualization, supervision. **D.E. Williams:** Conceptualization, writing–original draft. **S. Sathyanarayanan:** Conceptualization, resources, supervision, writing–original draft, project administration, writing–review and editing.

Acknowledgments

This study was funded by Codiak BioSciences.

The costs of publication of this article were defrayed in part by the payment of page charges. This article must therefore be hereby marked *advertisement* in accordance with 18 U.S.C. Section 1734 solely to indicate this fact.

Received June 11, 2020; revised October 5, 2020; accepted December 16, 2020; published first December 21, 2020.

References

1. Golomb HM, Jacobs A, Fefer A, Ozer H, Thompson J, Portlock C, et al. Alpha-2 interferon therapy of hairy-cell leukemia: a multicenter study of 64 patients. J Clin Oncol 1986;4:900–5.
2. Dutcher J. Current status of interleukin-2 therapy for metastatic renal cell carcinoma and metastatic melanoma. Oncology 2002;16: 4–10.
3. Liu J, Cao S, Kim S, Chung E, Homma Y, Guan X, et al. Interleukin-12: an update on its immunological activities, signaling and regulation of gene expression. Curr Immunol Rev 2005;1:119–37.
4. Watkins SK, Egilmez NK, Suttles J, Stout RD. IL12 rapidly alters the functional profile of tumor-associated and tumor-infiltrating macrophages in vitro and in vivo. J Immunol 2007;178:1357–62.

5. Shi X, Liu J, Xiang Z, Mitsuhashi M, Wu RS, Ma X. Gene expression analysis in interleukin-12-induced suppression of mouse mammary carcinoma. Int J Cancer 2004;110:570–8.
6. Kishima H, Shimizu K, Miyao Y, Mabuchi E, Tamura K, Tamura M, et al. Systemic interleukin 12 displays anti-tumour activity in the mouse central nervous system. Br J Cancer 1998;78:446–53.
7. Brunda MJ, Luistro L, Warrier RR, Wright RB, Hubbard BR, Murphy M, et al. Antitumor and antimetastatic activity of interleukin 12 against murine tumors. J Exp Med 1993;178:1223–30.
8. Brunda MJ, Luistro L, Rumennik L, Wright RB, Dvorozniak M, Aglione A, et al. Antitumor activity of interleukin 12 in preclinical models. Cancer Chemother Pharmacol 1996;38:S16–S21.
9. Lasek W, Zagożdżon R, Jakobisiak M. Interleukin. 12: still a promising candidate for tumor immunotherapy? Cancer Immunol Immunother 2014;63:419–35.
10. Rook AH, Wood GS, Yoo EK, Elenitsas R, Kao DMF, Sherman ML, et al. Interleukin-12 therapy of cutaneous T-cell lymphoma induces lesion regression and cytotoxic T-cell responses. Blood 1999;94:902–8.
11. Little RF, Pluda JM, Wyvill KM, Rodriguez-Chavez IR, Tosato G, Catanzaro AT, et al. Activity of subcutaneous interleukin-12 in AIDS-related Kaposi sarcoma. Blood 2006;107:4650–7.
12. Alatrash G, Hutson TE, Molto L, Richmond A, Nemec C, Mekhail T, et al. Clinical and immunologic effects of subcutaneously administered interleukin-12 and interferon alfa-2b: Phase I trial of patients with metastatic renal cell carcinoma or malignant melanoma. J Clin Oncol 2004;22:2891–900.
13. Cohen J. IL12 Deaths: explanation and a puzzle. Science 1995;270:908.
14. Car BD, Eng VM, Lipman JM, Anderson TD. The toxicology of interleukin-12: a review. Toxicol Pathol 1999;27:58–63.
15. Leonard JP, Sherman ML, Fisher GL, Buchanan LJ, Larsen G, Atkins MB, et al. Effects of single-dose interleukin-12 exposure on interleukin-12 associated toxicity and interferon-γ production. Blood 1997;90:2541–8.
16. Mahvi DM, Henry MB, Albertini MR, Weber S, Meredith K, Schalch H, et al. Intratumoral injection of IL12 plasmid DNA - Results of a phase I/IB clinical trial. Cancer Gene Ther 2007;14:717–23.
17. Heinzerling L, Burg G, Dummer R, Maier T, Oberholzer PA, Schultz J, et al. Intratumoral injection of DNA encoding human interleukin 12 into patients with metastatic melanoma: Clinical efficacy. Hum Gene Ther 2005;16:35–48.
18. Sangro B, Mazzolini G, Ruiz J, Herraiz M, Quiroga J, Herrero I, et al. Phase I trial of intratumoral injection of an adenovirus encoding interleukin-12 for advanced digestive tumors. J Clin Oncol 2004;22:1389–97.
19. Dooley K, Xu K, Haupt S, Lewis N, Harrison R, Martin S, et al. engEx: A novel exosome engineering platform enabling targeted transfer of pharmacological molecules [abstract].In: Proceedings of the American Association for Cancer Research Annual Meeting 2019; Mar 29–Apr 3; Atlanta, GA. Philadelphia (PA): AACR; 2019. Abstract nr 2150.
20. Kowal J, Arras G, Colombo M, Jouve M, Morath JP, Primdal-Bengtson B, et al. Proteomic comparison defines novel markers to characterize heterogeneous populations of extracellular vesicle subtypes. Proc Natl Acad Sci U S A 2016;113:E968–77.
21. Desai BB, Quinn PM, Wolitzky AG, Mongini PK, Chizzonite R, Gately MK. IL12 receptor. II. Distribution and regulation of receptor expression. J Immunol 1992;148:3125–32.
22. Zeh HJ, Perry-Lalley D, Dudley ME, Rosenberg SA, Yang JC. High avidity CTLs for two self-antigens demonstrate superior in vitro and in vivo antitumor efficacy. J Immunol 1999;162:989–94.
23. Jang SC, Moniz RJ, Sia CL, Harrison RA, Houde D, Ross N, et al. exoSTING: An engineered exosome therapeutic that selectively delivers STING agonist to the tumor resident antigen-presenting cells resulting in improved tumor antigen-specific adaptive immune response [abstract]. In: Proceedings of the American Association for Cancer Research Annual Meeting 2019; Mar 29–Apr 3; Atlanta, GA. Philadelphia (PA): AACR; 2019. Abstract nr 944.
24. Ross N, Dooley K, Ilovich O, Gottumukkala V, Houde D, Chan E, et al. Live imaging and biodistribution of 89Zr-labelled extracellular vesicles in rodents following intravenous, intraperitoneal, intrathecal, and intra-cisterna magna administration. J Extracell Vesicles 2017;6:1310414.
25. Basile LA, Ellefson D, Gluzman-Poltorak Z, Junes-Gill K, Mar V, Mendonca S, et al. Hemamax^{TM}, a recombinant human interleukin-12, is a potent mitigator of acute radiation injury in mice and non-human primates. PLoS One 2012;7:e30434.
26. Rudman SM, Jameson MB, McKeage MJ, Savage P, Jodrell DI, Harries M, et al. A phase 1 study of AS1409, a novel antibody-cytokine fusion protein, in patients with malignant melanoma or renal cell carcinoma. Clin Cancer Res 2011;17:1998–2005.
27. Momin N, Mehta NK, Bennett NR, Ma L, Palmeri JR, Chinn MM, et al. Anchoring of intratumorally administered cytokines to collagen safely potentiates systemic cancer immunotherapy. Sci Transl Med 2019;11:eaaw2614.
28. Mansurov A, Ishihara J, Hosseinchi P, Potin L, Marchell TM, Ishihara A, et al. Collagen-binding IL12 enhances tumour inflammation and drives the complete remission of established immunologically cold mouse tumours. Nat Biomed Eng 2020;4:531–43.
29. Strauss J, Heery CR, Kim JW, Jochems C, Donahue RN, Montgomery AS, et al. First-in-human phase I trial of a tumor-targeted cytokine (NHS-IL12) in subjects with metastatic solid tumors. Clin Cancer Res 2019;25:99–109.
30. Puca E, Probst P, Stringhini M, Murer P, Pellegrini G, Cazzamalli S, et al. The antibody-based delivery of interleukin-12 to solid tumors boosts NK and CD8+ T cell activity and synergizes with immune checkpoint inhibitors. Int J Cancer 2020;146:2518–30.
31. Chiocca EA, Yu JS, Lukas R V., Solomon IH, Ligon KL, Nakashima H, et al. Regulatable interleukin-12 gene therapy in patients with recurrent high-grade glioma: Results of a phase 1 trial. Sci Transl Med 2019;11:eaaw5680.
32. Bhatia S, Longino N V., Miller NJ, Kulikauskas R, Iyer JG, Ibrani D, et al. Intratumoral delivery of plasmid IL12 via electroporation leads to regression of injected and noninjected tumors in Merkel cell carcinoma. Clin Cancer Res 2020;26:598–607.
33. Greaney SK, Algazi AP, Tsai KK, Takamura KT, Chen L, Twitty CG, et al. Intratumoral plasmid IL12 electroporation therapy in patients with advanced melanoma induces systemic and intratumoral T-cell responses. Cancer Immunol Res 2020;8:246–54.
34. Van Herpen CM, Huijbens R, Looman M, De Vries J, Marres H, Van de Ven J, et al. Pharmacokinetics and immunological aspects of a phase Ib study with intratumoral administration of recombinant human interleukin-12 in patients with head and neck squamous cell carcinoma: A decrease of T-bet in peripheral blood mononuclear cells. Clin Cancer Res 2003;9:2950–6.
35. Rossowska J, Anger N, Wegierek K, Szczygieł A, Mierzejewska J, Milczarek M, et al. Antitumor potential of extracellular vesicles released by genetically modified murine colon carcinoma cells with overexpression of interleukin-12 and shRNA for TGF-β1. Front Immunol 2019;10:211.
36. Marabelle A, Andtbacka R, Harrington K, Melero I, Leidner R, de Baere T, et al. Starting the fight in the tumor: expert recommendations for the development of human intratumoral immunotherapy (HIT-IT). Ann Oncol 2018;29:2163–74.
37. Hather G, Liu R, Bandi S, Mettetal J, Manfredi M, Shyu W-C, et al. Growth rate analysis and efficient experimental design for tumor xenograft studies. Cancer Inform 2014;13:65–72.
38. Denney WS, Duvvuri S, Buckeridge C. Simple, automatic noncompartmental analysis: the PKNCA R package. J Pharmacokinet Pharmacodyn 2015;42:S65.